NANO LETTERS

Letter

pubs.acs.org/NanoLett

Pyrolysis of Cellulose under Ammonia Leads to Nitrogen-Doped Nanoporous Carbon Generated through Methane Formation

Wei Luo,[†] Bao Wang,[†] Christopher G. Heron,[†] Marshall J. Allen,[†] Jeff Morre,[†] Claudia S. Maier,[†] William F. Stickle,[‡] and Xiulei Ji*,[†]

[†]Department of Chemistry, Oregon State University, Corvallis, Oregon 97331, United States

[‡]Hewlett-Packard Co., 1000 NE Circle Blvd., Corvallis, Oregon 97330, United States

Supporting Information

ABSTRACT: Here, we present a simple one-step fabrication methodology for nitrogen-doped (N-doped) nanoporous carbon membranes via annealing cellulose filter paper under NH_3. We found that nitrogen doping (up to 10.3 at %) occurs during cellulose pyrolysis under NH_3 at as low as 550 °C. At 700 °C or above, N-doped carbon further reacts with NH_3, resulting in a large surface area (up to 1973.3 m^2/g). We discovered that the doped nitrogen, in fact, plays an important role in the reaction, leading to carbon gasification. CH_4 was experimentally detected by mass spectrometry as a product in the reaction between N-doped carbon and NH_3. When compared to conventional activated carbon (1533.6 m^2/g), the N-doped nanoporous carbon (1326.5 m^2/g) exhibits more than double the unit area capacitance (90 vs 41 mF/m^2).

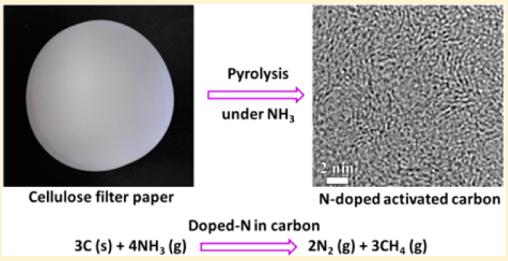

KEYWORDS: *Nanoporous carbon, NH_3 activation, nitrogen doping, methane formation*

Activated carbons (ACs) are strategically important in energy storage[1−4] and environmental protection applications[5] due to their low cost and high porosity and scalability. Fabrication process of ACs from raw materials, such as petroleum pitch or biomass, typically consists of two separate steps: pyrolysis and activation.[6] During the first process, oxygen and hydrogen contents in precursors are mostly eliminated, and carbons with modest surface areas are constructed.[7,8] The following activation process creates porosity by reacting carbon with oxidants at elevated temperatures. The oxidants can be gaseous ones, e.g., CO_2[9] and H_2O,[10] or molten salts, e.g., KOH[11−13] and $ZnCl_2$.[14] It is widely believed that the activation step requires carbon oxidation, while a large porosity created in ACs by a reductant has been rarely reported.

Recently, N-doped carbonaceous materials have raised increasing interest due to their improved properties in electronics,[15] catalysis,[16,17] CO_2 adsorption,[18] batteries,[19,20] and electrical double-layer capacitors (EDLCs),[21,22] compared with their pure carbon counterparts. For preparation of these materials, one approach is to use nitrogen-containing organic precursors[23−25] or ionic liquids[26,27] for pyrolysis. By controlling the pyrolysis conditions, the as-prepared carbons can possess a high nitrogen content, e.g., 40 wt % in carbon derived from 1-ethyl-3-methylimidazolium. Chemical vapor deposition has also been investigated to synthesize N-doped carbon nanotubes[28−32] or graphene,[33−35] which realizes direct incorporation of nitrogen atoms into carbon and leads to superior physicochemical properties. As another strategy, reacting graphene oxide with nitrogen-containing salts under hydrothermal conditions can form N-doped reduced graphene oxide materials.[36−41] These N-doped reduced graphene materials exhibit much better dispersion in solvents, which is critical for applications. Other methods, including solvothermal reactions, arc discharge, and plasma treatment, have also been employed to form N-doped graphene materials.[42,43] Another important approach is to anneal carbon materials under NH_3 gas[44−46] or NH_3/steam mixture[47,48] at elevated temperatures. Reactions between NH_3 and carbonaceous materials at temperatures lower than 1000 °C can enable a certain level of nitrogen doping. However, a carbon burnoff or significantly increased specific surface/pore volume has not been reported for annealing carbon under NH_3.[49]

NH_3 has long been used as a flowing gas in forming metal nitrides by annealing nitrogen-containing organometallic compounds. Interestingly, much less carbon residue remains after the pyrolysis under NH_3 than the cases under N_2 or Ar, which suggests carbon gasification under NH_3.[50,51] This is very much different from the pyrolysis of pure carbon under NH_3. Unfortunately, not much attention has been paid to this phenomenon, and the mechanism has yet to be explored. It seems to us that there might be a certain reactive mechanism involved for carbon gasification during the pyrolysis of these precursors. However, the raw materials of organometallic compounds in previous studies are too special to reveal the mechanism.

Herein, we study the pyrolysis of cellulose, the most abundant polymer, under NH_3 to uncover the burnoff

Received: March 6, 2014
Revised: March 18, 2014
Published: March 28, 2014

 © 2014 American Chemical Society dx.doi.org/10.1021/nl500859p | *Nano Lett.* 2014, 14, 2225−2229

mechanism. We, for the first time, demonstrate that N-doped activated carbon (NAC) membranes with large surface areas can be prepared in a one-step fabrication by heating cellulose filter paper (CFP) under NH_3, a reducing activation agent. The specific surface area and nitrogen content of NACs can be readily tuned by varying the experimental conditions. Moreover, we experimentally confirmed the formation of CH_4 from the NH_3 activation reaction with N-doped carbon. We also discovered the doped nitrogen plays an important role in the activation reaction of carbon under NH_3. More importantly, the N-doped carbon membrane exhibits good performance in EDLCs as binder-free electrodes.

A series of NAC membranes with different specific surface areas and nitrogen contents have been synthesized by annealing CFP under NH_3. When CFP was heated under NH_3 at T °C for X h, the obtained NAC is referred to as NAC-T-Xh (Table 1). All obtained samples except NAC-1000-2h exhibit excellent

Table 1. Burnoff, Specific Surface Area, And Chemical Compositions of NACs and Ar-1000-2h

sample no.	burnoff (wt %)	S_{BET} (m^2/g)	XPS C (at %)	XPS O (at %)	XPS N (at %)
NAC-550-2h	40.9	93.3	84.5	6.5	9.0
NAC-550-6h	62.4	91.8	84.1	5.6	10.3
NAC-700-2h	69.5	390.6	85.3	4.7	10.0
NAC-700-6h	71.1	544.4	85.1	4.7	10.2
NAC-850-2h	84.2	889.2	91.7	3.8	4.5
NAC-850-6h	89.4	1326.5	93.3	2.5	4.2
NAC-1000-2h	98.3	1973.3	94.1	4.0	1.9
Ar-1000-2h	64.0	302.2	97.8	2.2	0

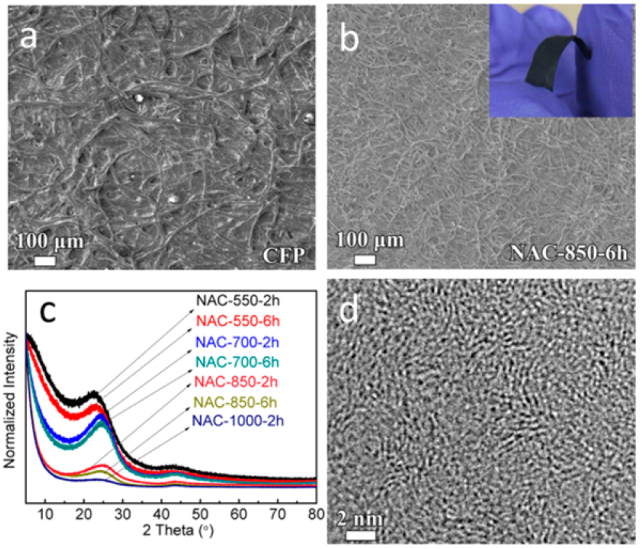

Figure 1. SEM images of (a) CFP and (b) NAC-850-6h. Inset of (b): a digital image of NAC-850-6h. (c) XRD patterns of NACs. (d) A HRTEM image of NAC-850-6h.

membrane flexibility, as indicated in Figure 1b inset. The morphology of membranes was well maintained after the heat treatment, as shown in scanning electron microscopy (SEM) images (Figures 1a,b and S1). The carbon lattice structure in NACs was studied by X-ray diffraction (XRD) patterns (Figure 1c). By comparing the intensity of (002) peaks, it is evident that the graphitization degrees of NACs first increases from 550 to 700 °C then decreases sharply at higher temperatures of 850 and 1000 °C. A representative high-resolution transmission electron microscopy (HRTEM) image reveals a typical amorphous carbon lattice where tiny graphite domains consisting of 2−3 layers of graphene sheets exist in NAC-850-6h (Figure 1d).

In Raman spectra, all NACs exhibit two characteristic bands at ~1350 cm^{-1} (D-band) and ~1580 cm^{-1} (G-band) that can be assigned to carbon sp^3 and sp^2 configuration, respectively (Figure 2a). Surprisingly, the intensity ratios of D- and G-bands (I_D/I_G) are below 1.0 for NACs formed at 550 °C, indicative of a high graphitization degree. The I_D/I_G ratio increases upon higher annealing temperatures and longer durations, suggesting more disordered structures. Note a higher pyrolysis temperature typically leads to a higher degree of graphitization under an inert gas atmosphere, while the opposite is observed under NH_3. The more amorphous structure obtained at higher temperatures should be attributed to an activation process under NH_3 that will be further discussed later on.

N_2 sorption measurements for NACs were carried out. For the purposes of comparison, a reference carbon, designated as Ar-1000-2h, was also prepared by annealing CFP in Ar at 1000 °C for 2 h. As shown in Figure 2b, all NACs exhibit Type I isotherms, indicative of microporous structures. It is evident that specific surface areas and pore volumes rise along with higher heating temperatures and longer durations during pyrolysis. As summarized in Table 1, calculations based on the isotherms give Brumauer−Emmett−Teller (BET) surface areas of 93.3 and 91.8 m^2/g for NAC-550-2h and NAC-550-6h, respectively. The low specific surface areas suggest that little activation occurs at this temperature. At 700 °C, the specific surface areas rise to 390.6 and 544.4 m^2/g for NAC-700-2h and NAC-700-6h, respectively. Note that Ar-1000-2h exhibits a lower BET surface area of 302.2 m^2/g than NAC-700-2h. This clearly indicates that carbon activation process under NH_3 occurs at as low as 700 °C. At higher temperatures of 850 and 1000 °C, the surface areas reach 889.2, 1326.5, and 1973.3 m^2/g for NAC-850-2h, NAC-850-6h, and NAC-1000-2h, respectively. This further demonstrates the activation effect under NH_3 and corroborates the lower graphitization degrees of these NACs revealed by XRD and Raman measurements. We also carefully recorded the burnoff for every experiment, as summarized in Table 1. Under NH_3, the burnoff increases upon higher heating temperatures and longer durations and reached 89.4 wt % for NAC-850-6h, compared to 64.0 wt % for Ar-1000-2h. X-ray photoelectron spectrometer (XPS) was further employed to characterize the chemical composition of NACs obtained under various conditions (Figure 2c and Table 1). As a reference, Ar-1000-2h consists of 97.8 at % carbon and 2.2 at % oxygen, which indicates an effective carbonization. Under NH_3, N-doping occurs through the reaction of NH_3 with the oxygenated species in the cellulose.[49,52,53] At 550 °C, nitrogen constitutes 9.0 and 10.3 at % in NAC-550-2h and NAC-550-6h, respectively. At 700 °C, nitrogen content is stabilized at around 10.0 at % in NAC-700-2h and NAC-700-6h. However, at even higher temperatures of 850 and 1000 °C, nitrogen content drops to 4.5 at % for NAC-850-2h, 4.2 at % for NAC-850-6h, and 1.9 at % for NAC-1000-2h, which should be due to the effective removal of oxygenated species at a high temperature. For example, oxygen in NAC-850-6h is only 2.5 at %, comparable to that of Ar-1000-2h. Furthermore, the high-resolution XPS spectra of N 1s were collected to understand

dx.doi.org/10.1021/nl500859p | Nano Lett. 2014, 14, 2225−2229

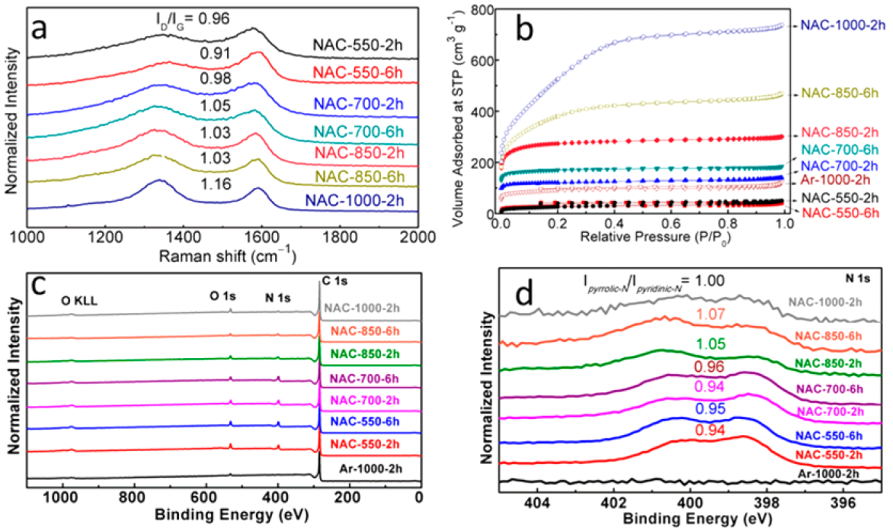

Figure 2. (a) Raman spectra and (b) N_2 sorption isotherms of NACs and Ar-1000-2h. XPS spectra of NACs and Ar-1000-2h: (c) survey spectra and (d) high-resolution N 1s spectra.

the formed N-carbon bonding under NH_3 (Figure 2d). The N 1s signal can be deconvoluted into two components corresponding to pyrrolic-N (400.7 eV) and pyridinic-N (398.3 eV), respectively.[24,46] It is evident that the doped nitrogen atoms are bonded within the carbon lattice instead of dangling on the carbon surface. The intensity ratio of pyrrolic-N and pyridinic-N peaks gradually increases upon higher annealing temperature and longer durations, which suggests the activation is more likely at the expense of aromatic rings than N-containing five-membered rings.

It is important to reveal the activation mechanism of cellulose-derived carbon under NH_3. As listed in Table 1, a longer annealing duration (6 vs 2 h) at 850 °C results in a higher burnoff (89.4 vs 84.2 wt %) and a larger specific surface area (1326.5 vs 889.2 m^2/g). Inspired by the reports on the more reactivity of N-doped carbon,[16,17] we did a simple experiment to test whether it is the doped nitrogen that results in the activation process. Both N-free carbon (Ar-1000-2h) and N-doped carbon (NAC-850-2h, 4.5 at % of N) were annealed under NH_3 at 850 °C for 1 h. A weight loss of ~5% was observed for Ar-1000-2h, while the burnoff is about 50 wt % for NAC-850-2h. The vast burnoff difference unequivocally confirms that doped nitrogen in NAC-850-2h plays an important role on the activation reactions between carbon and NH_3.

In order to further investigate the mechanism, mass spectrometry (MS) was used to analyze the exhaust gas collected after the furnace temperature had risen to 850 °C for 2 h when the formation process of NAC-850-2h is nearly finished. The spectra of the exhaust gas, background, and methane standard are shown in Figure 3. In contrast to the background, exhaust gas, and methane standard share similar peaks, particularly, at mass/charge ratios of 15 and 29 that are assigned to CH_3^+ and $CH_3CH_2^+$ from the CH_4 plasma. This proves the CH_4 production during the activation process. It is well-known that the decomposition of organic compounds does not generate CH_4.[7,8] Our results, for the first time, experimentally confirm the CH_4 formation from the reaction between NH_3 and N-doped carbon. Here, we postulate an activation mechanism that can be described by the following equation:

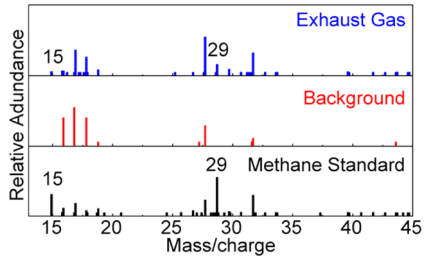

Figure 3. MS study on exhaust gas from the activation reaction. A spectrum of exhaust gas collected after the reaction temperature had risen to 850 °C for 2 h during the formation of NAC-850-2h (up, blue), a background spectrum of air (middle, red), and a standard methane spectrum (down, black).

$$3C(s) + 4NH_3(g) \xrightarrow{\text{doped-N in carbon}} 2N_2(g) + 3CH_4(g)$$

Considering more defects and different electronic structure of carbon due to the N-doping, it is possible that N_2 is formed by the nitrogen from NH_3 and the doped nitrogen in carbon. Further mechanistic study is undergoing to confirm this postulation.

N-doping is one of the most promising strategies to enhance the performance of carbon electrodes in EDLCs. We investigated NAC-850-6h as a free-standing binder-free electrode in EDLCs with a basic aqueous electrolyte (2.0 M KOH). NAC-850-6h was chosen due to its high surface area and good membrane integrity. A series of cyclic voltammograms (CV) of NAC-850-6h at different scanning rates reveal a typical capacitive behavior (Figure 4a). Figure 4b shows the galvanostatic charge/discharge profiles of NAC-850-6h at a current rate of 1.0 A/g, where a specific capacitance of ~120 F/g is calculated. In a control experiment, a conventional activated carbon (CAC), obtained by activating a coal-derived carbon under CO_2 at 860 °C for 22.5 h, was also investigated. As shown in Figure 4b, CAC shows a much lower capacitance of 63 F/g with an even higher surface area of 1533.6 m^2/g (Figure S2) than NAC-850-6h (1326.5 m^2/g). NAC-850-6h exhibits more than double the unit area capacitance than CAC (90 vs 41 mF/m^2). Additionally, electrochemical impedance spectroscopy (EIS) measurements were conducted (Figure 4c,d). The

dx.doi.org/10.1021/nl500859p | Nano Lett. 2014, 14, 2225−2229

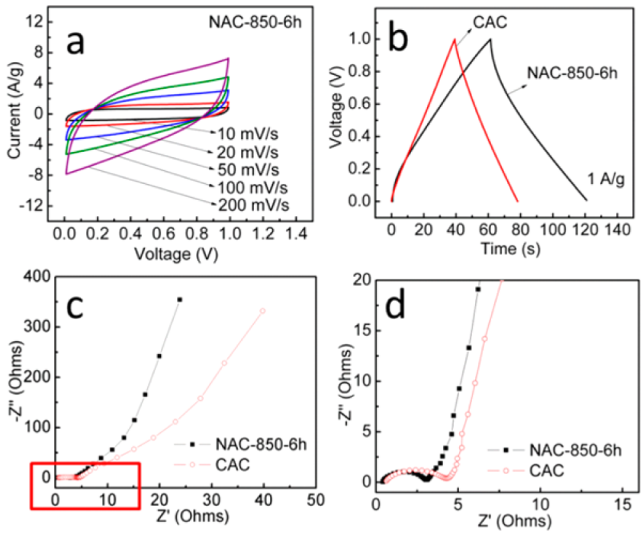

Figure 4. (a) CV curves of NAC-850-6h at different scan rates. (b) Galvanostatic charge/discharge profiles of NAC-850-6h and CAC at a current density of 1.0 A/g. (c) Nyquist plots of NAC-850-6h and CAC, and (d) an enlarged Nyquist plots corresponding to the red square marked area in (c).

Nyquist plots of both NAC-850-6h and CAC show a semicircle followed by a sloping straight line. NAC-850-6h exhibits a slightly lower intercept (0.4 Ω) at the real impedance (Z′) axis in the high-frequency region than CAC (0.6 Ω), indicating a smaller internal resistance. A smaller diameter of the semicircle from NAC-850-6h reveals a less charge-transfer resistance on the electrode surface than CAC. The less resistance should be attributed to the N-doping in the carbon structure. A much higher slope at the low-frequency region clearly shows a much better pore accessibility for electrolyte in NAC-850-6h than CAC,[54] which may be due to the N-doping enhanced hydrophilicity. Our results suggest that the simple approach of activating cellulose under NH_3 can be a facile methodology to manufacture advanced electrode materials for EDLCs.

In conclusion, we have introduced the following discoveries in this study: (i) N-doped activated carbon membranes with tunable nitrogen contents and surface areas can be formed by annealing cellulose filter paper under NH_3; (ii) doped nitrogen in carbon lattice plays an important role in the activation reaction of carbon under NH_3; and (iii) methane is formed as a product in the reactions between N-doped carbon and NH_3.

■ ASSOCIATED CONTENT

Supporting Information

Experimental section, characterization details, and supporting data. This material is available free of charge via the Internet at http://pubs.acs.org.

■ AUTHOR INFORMATION

Corresponding Author

*E-mail: David.Ji@oregonstate.edu.

Notes

The authors declare no competing financial interest.

■ ACKNOWLEDGMENTS

X.J. gratefully acknowledges the financial support from Oregon State University. We thank Dr. Peter Eschbach and Ms. Teresa Sawyer for the SEM measurements in OSU Electron Microscopy Facility. We are thankful to Mr. Joshua Razink for the TEM measurements at the Center for Advanced Materials Characterization at Oregon (CAMCOR). We appreciate Professor Chih-Hung Chang and Mr. Changqing Pan for Raman analysis.

■ REFERENCES

(1) Simon, P.; Gogotsi, Y. *Acc. Chem. Res.* **2013**, *46*, 1094−1103.
(2) Simon, P.; Gogotsi, Y. *Nat. Mater.* **2008**, *7*, 845−854.
(3) Zhai, Y.; Dou, Y.; Zhao, D.; Fulvio, P. F.; Mayes, R. T.; Dai, S. *Adv. Mater.* **2011**, *23*, 4828−4850.
(4) Miller, J. R.; Burke, A. F. *Electrochem. Soc. Interface* **2008**, *17*, 53−57.
(5) Yang, K.; Xing, B. *Chem. Rev.* **2010**, *110*, 5989−6008.
(6) Noked, M.; Soffer, A.; Aurbach, D. *J. Solid State Electrochem.* **2011**, *15*, 1563−1578.
(7) Lin, Y.-C.; Cho, J.; Tompsett, G. A.; Westmoreland, P. R.; Huber, G. W. *J. Phys. Chem. C* **2009**, *113*, 20097−20107.
(8) Lin, T.; Goos, E.; Riedel, U. *Fuel Process. Technol.* **2013**, *115*, 246−253.
(9) Rodríguez-Reinoso, F.; Molina-Sabio, M.; González, M. T. *Carbon* **1995**, *33*, 15−23..
(10) Molina-Sabio, M.; Gonzalez, M. T.; Rodriguez-Reinoso, F.; Sepulveda-Escribano, A. *Carbon* **1996**, *34*, 505−509.
(11) Lv, Y.; Zhang, F.; Dou, Y.; Zhai, Y.; Wang, J.; Liu, H.; Xia, Y.; Tu, B.; Zhao, D. *J. Mater. Chem.* **2012**, *22*, 93−99.
(12) Wei, L.; Sevilla, M.; Fuertes, A. B.; Mokaya, R.; Yushin, G. *Adv. Funct. Mater.* **2012**, *22*, 827−834.
(13) Zhao, L.; Fan, L.-Z.; Zhou, M.-Q.; Guan, H.; Qiao, S.; Antonietti, M.; Titirici, M.-M. *Adv. Mater.* **2010**, *22*, 5202−5206.
(14) Khalili, N. R.; Campbell, M.; Sandi, G.; Golaś, J. *Carbon* **2000**, *38*, 1905−1915.
(15) Wang, X.; Li, X.; Zhang, L.; Yoon, Y.; Weber, P. K.; Wang, H.; Guo, J.; Dai, H. *Science* **2009**, *324*, 768−771.
(16) Gong, K.; Du, F.; Xia, Z.; Durstock, M.; Dai, L. *Science* **2009**, *323*, 760−764.
(17) Maldonado, S.; Stevenson, K. J. *J. Phys. Chem. B* **2005**, *109*, 4707−4716.
(18) Nandi, M.; Okada, K.; Dutta, A.; Bhaumik, A.; Maruyama, J.; Derks, D.; Uyama, H. *Chem. Commun.* **2012**, *48*, 10283−10285.
(19) Shao, Y.; Wang, X.; Engelhard, M.; Wang, C.; Dai, S.; Liu, J.; Yang, Z.; Lin, Y. *J. Power Sources* **2010**, *195*, 4375−4379.
(20) Li, Y.; Wang, J.; Li, X.; Liu, J.; Geng, D.; Yang, J.; Li, R.; Sun, X. *Electrochem. Commun.* **2011**, *13*, 668−672.
(21) Zhang, L. L.; Zhao, X.; Ji, H.; Stoller, M. D.; Lai, L.; Murali, S.; McDonnell, S.; Cleveger, B.; Wallace, R. M.; Ruoff, R. S. *Energy Environ. Sci.* **2012**, *5*, 9618−9625.
(22) Chen, P.; Xiao, T.-Y.; Qian, Y.-H.; Li, S.-S.; Yu, S.-H. *Adv. Mater.* **2013**, *25*, 3192−3196.
(23) Wang, Z.; Qie, L.; Yuan, L.; Zhang, W.; Hu, X.; Huang, Y. *Carbon* **2013**, *55*, 328−334.
(24) Qie, L.; Chen, W.; Wang, Z.; Shao, Q.; Li, X.; Yuan, L.; Hu, X.; Zhang, W.; Huang, Y. *Adv. Mater.* **2012**, *24*, 2047−2050.
(25) Qie, L.; Chen, W.; Xu, H.; Xiong, X.; Jiang, Y.; Zou, F.; Hu, X.; Xin, Y.; Zhang, Z.; Huang, Y. *Energy Environ. Sci.* **2013**, *6*, 2497−2504.
(26) Wang, X.; Dai, S. *Angew. Chem., Int. Ed.* **2010**, *49*, 6664−6668.
(27) Paraknowitsch, J. P.; Zhang, J.; Su, D.; Thomas, A.; Antonietti, M. *Adv. Mater.* **2010**, *22*, 87−92.
(28) Maldonado, S.; Morin, S.; Stevenson, K. J. *Carbon* **2006**, *44*, 1429−1437.
(29) Chen, Z.; Higgins, D.; Tao, H.; Hsu, R. S.; Chen, Z. *J. Phys. Chem. C* **2009**, *113*, 21008−21013.
(30) Wiggins-Camacho, J. D.; Stevenson, K. J. *J. Phys. Chem. C* **2009**, *113*, 19082−19090.
(31) Chen, Z.; Higgins, D.; Chen, Z. *Carbon* **2010**, *48*, 3057−3065.
(32) Chen, Z.; Yu, A.; Higgins, D.; Li, H.; Wang, H.; Chen, Z. *Nano Lett.* **2012**, *12*, 1946−1952.

(33) Qu, L.; Liu, Y.; Baek, J.-B.; Dai, L. *ACS Nano* **2010**, *4*, 1321−1326.
(34) Wei, D.; Liu, Y.; Wang, Y.; Zhang, H.; Huang, L.; Yu, G. *Nano Lett.* **2009**, *9*, 1752−1758.
(35) Wang, Y.; Shao, Y.; Matson, D. W.; Li, J.; Lin, Y. *ACS Nano* **2010**, *4*, 1790−1798.
(36) Liang, Y.; Li, Y.; Wang, H.; Zhou, J.; Wang, J.; Regier, T.; Dai, H. *Nat. Mater.* **2011**, *10*, 780−786.
(37) Liang, Y.; Wang, H.; Zhou, J.; Li, Y.; Wang, J.; Regier, T.; Dai, H. *J. Am. Chem. Soc.* **2012**, *134*, 3517−3523.
(38) Park, S.; Hu, Y.; Hwang, J. O.; Lee, E.-S.; Casabianca, L. B.; Cai, W.; Potts, J. R.; Ha, H.-W.; Chen, S.; Oh, J.; Kim, S. O.; Kim, Y.-H.; Ishii, Y.; Ruoff, R. S. *Nat. Commun.* **2012**, *3*, 638.
(39) Hasan, S. A.; Tsekoura, E. K.; Sternhagen, V.; Strømme, M. *J. Phys. Chem. C* **2012**, *116*, 6530−6536.
(40) Long, D.; Li, W.; Ling, L.; Miyawaki, J.; Mochida, I.; Yoon, S.-H. *Langmuir* **2010**, *26*, 16096−16102.
(41) Chen, P.; Xiao, T.-Y.; Li, H.-H.; Yang, J.-J.; Wang, Z.; Yao, H.-B.; Yu, S.-H. *ACS Nano* **2011**, *6*, 712−719.
(42) Raymundo-Piñero, E.; Cazorla-Amorós, D.; Linares-Solano, A. *Carbon* **2003**, *41*, 1925−1932.
(43) Wang, H.; Maiyalagan, T.; Wang, X. *ACS Catal.* **2012**, *2*, 781−794.
(44) Mangun, C. L.; Benak, K. R.; Economy, J.; Foster, K. L. *Carbon* **2001**, *39*, 1809−1820.
(45) Wu, Z.-S.; Ren, W.; Xu, L.; Li, F.; Cheng, H.-M. *ACS Nano* **2011**, *5*, 5463−5471.
(46) Xue, Y.; Liu, J.; Chen, H.; Wang, R.; Li, D.; Qu, J.; Dai, L. *Angew. Chem., Int. Ed.* **2012**, *51*, 12124−12127.
(47) Boudou, J. P. *Carbon* **2003**, *41*, 1955−1963.
(48) Boudou, J. P.; Chehimi, M.; Broniek, E.; Siemieniewska, T.; Bimer, J. *Carbon* **2003**, *41*, 1999−2007.
(49) Li, X.; Wang, H.; Robinson, J. T.; Sanchez, H.; Diankov, G.; Dai, H. *J. Am. Chem. Soc.* **2009**, *131*, 15939−15944.
(50) Paciorek, K. J.; Kratzer, R. H.; Harris, D. H.; Smythe, M. E.; Kimble, P. F. US Patent 4,581,468, 1986.
(51) Jiang, Z.; Interrante, L. V. *Chem. Mater.* **1990**, *2*, 439−446.
(52) Arrigo, R.; Havecker, M.; Schlogl, R.; Su, D. S. *Chem. Commun.* **2008**, *40*, 4891−4893.
(53) Arrigo, R.; Havecker, M.; Wrabetz, S.; Blume, R.; Lerch, M.; McGregor, J.; Parrott, E. P. J.; Zeitler, J. A.; Gladden, L. F.; Knop-Gericke, A.; Schlögl, R.; Su, D. S. *J. Am. Chem. Soc.* **2010**, *132*, 9616−9630.
(54) Huang, C.-H.; Zhang, Q.; Chou, T.-C.; Chen, C.-M.; Su, D. S.; Doong, R.-A. *ChemSusChem* **2012**, *5*, 563−571.